REPORT DOCUMENTATION PAGE

Form Approved
OMB No. 0704-0188

Public reporting burden for this collection of information is estimated to average 1 hour per response, including the time for reviewing instructions, searching existing data sources, gathering and maintaining the data needed, and completing and reviewing this collection of information. Send comments regarding this burden estimate or any other aspect of this collection of information, including suggestions for reducing this burden to Department of Defense, Washington Headquarters Services, Directorate for Information Operations and Reports (0704-0188), 1215 Jefferson Davis Highway, Suite 1204, Arlington, VA 22202-4302. Respondents should be aware that notwithstanding any other provision of law, no person shall be subject to any penalty for failing to comply with a collection of information if it does not display a currently valid OMB control number. **PLEASE DO NOT RETURN YOUR FORM TO THE ABOVE ADDRESS.**

1. REPORT DATE *(DD-MM-YYYY)*	**2. REPORT TYPE**	**3. DATES COVERED** *(From - To)*
29-05-2007	Technical Paper	

4. TITLE AND SUBTITLE

Thrust Efficiency, Energy Efficiency, and the Role of VDF in Hall Thruster Performance Analysis (Postprint)

5a. CONTRACT NUMBER

5b. GRANT NUMBER

5c. PROGRAM ELEMENT NUMBER

6. AUTHOR(S)
C. William Larson & William A. Hargus (AFRL/PRSS); Daniel L. Brown (ERC)

5d. PROJECT NUMBER
33SP0708

5e. TASK NUMBER

5f. WORK UNIT NUMBER

7. PERFORMING ORGANIZATION NAME(S) AND ADDRESS(ES)

Air Force Research Laboratory (AFMC)
AFRL/PRSS
1 Ara Drive
Edwards AFB CA 93524-7013

8. PERFORMING ORGANIZATION REPORT NUMBER

AFRL-PR-ED-TP-2007-316

9. SPONSORING / MONITORING AGENCY NAME(S) AND ADDRESS(ES)

Air Force Research Laboratory (AFMC)
AFRL/PRS
5 Pollux Drive
Edwards AFB CA 93524-70448

10. SPONSOR/MONITOR'S ACRONYM(S)

11. SPONSOR/MONITOR'S NUMBER(S)
AFRL-PR-ED-TP-2007-316

12. DISTRIBUTION / AVAILABILITY STATEMENT

Approved for public release; distribution unlimited (07207A)

13. SUPPLEMENTARY NOTES
AIAA 2007-5270. Presented at the 43rd AIAA/ASME/SAE/ASEE Joint Propulsion Conference, Cincinnati, OH, 8-11 July 2007.

14. ABSTRACT A rocket power efficiency equation was written to explicitly account for the effect of the velocity distribution function (VDF) of the propellant jet on the conversion of anode electrical energy to jet kinetic energy. This enabled a mathematically rigorous distinction to be made between thrust efficiency and energy efficiency. In this approach anode thrust efficiency, the commonly reported figure of merit for Hall thrusters, is the product of three utilization efficiencies: (1) propellant utilization efficiency, (2) voltage utilization efficiency, and (3) current utilization efficiency, which are less than unity under all real operating conditions. Unit propellant utilization is characterized by 100 percent ionization to a single ionic species whose thrust vectors are all directed along the same thrust axis. Anode voltage utilization efficiency is unity when ion species are created at the anode and accelerated through the entire anode potential. Current utilization efficiency is the fraction of cathode electron flow utilized in neutralization of accelerated positive ions. It can never be unity because a portion of the electron flow must be recycled back to the anode to provide energy to ionize neutral propellant. The architecture of the efficiency analysis is such that energy efficiency becomes naturally expressed as a product of voltage and current utilization efficiencies, and is rigorously separated from propellant utilization efficiency. Thus, thrust efficiency is the product of propellant utilization efficiency and energy efficiency. The methodology is applied to analysis of data from systematic low and high power (0.2 to 50 kW) Hall thruster performance studies published in the open literature. The cited data includes measurement of thrust, propellant mass flow rate, anode voltage, and anode current coupled with various electrical and optical diagnostics that provide information about the VDF and thermodynamic state of the propellant jet.

15. SUBJECT TERMS

16. SECURITY CLASSIFICATION OF:			**17. LIMITATION OF ABSTRACT**	**18. NUMBER OF PAGES**	**19a. NAME OF RESPONSIBLE PERSON**
					Dr. James Haas
a. REPORT	**b. ABSTRACT**	**c. THIS PAGE**	SAR	19	**19b. TELEPHONE NUMBER** *(include area code)*
Unclassified	**Unclassified**	**Unclassified**			N/A

43rd AIAA/ASME/SAE/ASEE Joint Propulsion Conference & Exhibit
8 - 11 July 2007, Cincinnati, OH

AIAA 2007-5270

Thrust Efficiency, Energy Efficiency and the Role of VDF in Hall Thruster Performance Analysis*

C. William Larson[1], Daniel L. Brown[2], and William A. Hargus, Jr.[3]
Air Force Research Laboratory, Edwards AFB, CA 93524-7680

[Abstract] A rocket power efficiency equation was written to explicitly account for the effect of the velocity distribution function (VDF) of the propellant jet on the conversion of anode electrical energy to jet kinetic energy. This enabled a mathematically rigorous distinction to be made between thrust efficiency and energy efficiency. In this approach anode thrust efficiency, the commonly reported figure of merit for Hall thrusters, is the product of three utilization efficiencies: (1) propellant utilization efficiency, (2) voltage utilization efficiency, and (3) current utilization efficiency, which are less than unity under all real operating conditions. Unit propellant utilization is characterized by 100 percent ionization to a single ionic species whose thrust vectors are all directed along the same thrust axis. Anode voltage utilization efficiency is unity when ion species are created at the anode and accelerated through the entire anode potential. Current utilization efficiency is the fraction of cathode electron flow utilized in neutralization of accelerated positive ions. It can never be unity because a portion of the electron flow must be recycled back to the anode to provide energy to ionize neutral propellant. The architecture of the efficiency analysis is such that energy efficiency becomes naturally expressed as a product of voltage and current utilization efficiencies, and is rigorously separated from propellant utilization efficiency. Thus, thrust efficiency is the product of propellant utilization efficiency and energy efficiency. The methodology is applied to analysis of data from systematic low and high power (0.2 to 50 kW) Hall thruster performance studies published in the open literature. The cited data includes measurement of thrust, propellant mass flow rate, anode voltage, and anode current coupled with various electrical and optical diagnostics that provide information about the VDF and thermodynamic state of the propellant jet. At their optimum operating points all Hall thrusters appear to require ~ 10% to 30% of the total electron flow to be recycled through the plasma to ionize propellant and sustain the plasma processes. Recycled electrons loose their energy by ionizing neutrals and by joule heating. It appears that anode thrust efficiencies in the neighborhood of 75% that have been achieved in higher power thrusters (> ~ 5 kW, operating with xenon and producing thrust to power ratio ~ 50 mN/kW at specific impulse ~ 3000 seconds), may be nearing a practical upper limit as this requires a geometric mean of the three utilization efficiencies of around 91%.

*Distribution A – Approved for Public Release, Distribution Unlimited.

[1]Research Scientist, Spacecraft Propulsion Branch, AFRL/PRSS, AIAA Member.
[2]PhD Candidate, Univ. of Michigan Plasmadynamics and Electric Propulsion Laboratory, AIAA Student Member.
[3]Research Scientist, Spacecraft Propulsion Branch, AFRL/PRSS, AIAA Member.

This material is declared a work of the U.S. Government and is not subject to copyright protection in the United States.

Nomenclature (In order of usage)

η_{thrust} = experimental thrust efficiency.
$\mathbf{F}$ = measured thrust vector.
V_a = measured anode voltage.
I_a = measured anode current.
P_{in} = input power to anode.
$\dot{m}$ = measured propellant mass flow rate.
$\langle \mathbf{v} \rangle$ = mass weighted average exit velocity, specific impulse.
g_o = Earth's gravitational constant at sea level, 9.806 m/s^2.
I_{sp} = specific impulse, independent of unit system, $I_{sp} = \langle \mathbf{v} \rangle / g_o$.
u_{in} = specific energy input = $P_{in}/\dot{m} = P_{in}/[\mathbf{F}/\langle v \rangle] = \langle \mathbf{v} \rangle / [\mathbf{F}/P_{in}]$.
$\langle \mathbf{v}^2 \rangle$ = mass weighted average squared exit velocity.
P_{jet} = power of jet = $\frac{1}{2} \dot{m} \langle \mathbf{v}^2 \rangle$.
η_{energy} = energy efficiency = P_{jet}/P_{in}.
Φ = Phi Factor = $\langle \mathbf{v} \rangle^2 / \langle \mathbf{v}^2 \rangle$, propellant utilization efficiency.
Φ_{vdf} = Phi factor for VDF loss.
Φ_{div} = Phi factor for divergence loss.
α = plume momentum divergence half angle.
f_0, f_1, f_2, f_3 = exit mass fractions of $Xe^0, Xe^{+1}, Xe^{+2}, Xe^{+3}$ where $f_0 + f_1 + f_2 + f_3 = 1$.
$\mathbf{v}_0, \mathbf{v}_1, \mathbf{v}_2, \mathbf{v}_3$ = exit velocities of $Xe^0, Xe^{+1}, Xe^{+2}, Xe^{+3}$.
r_0, r_2, r_3 = velocity ratios, $\mathbf{v}_0/\mathbf{v}_1$, $\mathbf{v}_2/\mathbf{v}_1$, $\mathbf{v}_3/\mathbf{v}_1$.
f_i = ion mass fraction at exit = $f_1+f_2+f_3$.
f^*_1, f^*_2, f^*_3 = reduced ion mass fractions at exit, $f^*_1+f^*_2+f^*_3=1$, $f^*_1=f_1/f_i$, $f^*_2=f_2/f_i$, $f^*_3=f_3/f_i$.
a = quality factor of VDF, $a = \Phi_{vdf}/f_i$.
$\mathscr{F}$ = Faraday constant, 96485 coulombs/mol of charge.
$\mathscr{M}$ = molecular weight of propellant, xenon = 0.1313 kg/mol, krypton = 0.08380 kg/mol.
$\langle \mathbf{v}^2 \rangle_+$ = average squared velocity of ion species = $f^*_1 \mathbf{v}_1^2 + f^*_2 \mathbf{v}_2^2 + f^*_3 \mathbf{v}_3^2$.
Q = average charge of ion species = $f^*_1 + 2f^*_2 + 3f^*_3$.
$\delta V_1, \delta V_2, \delta V_3$ = acceleration voltages of $Xe^{+1}, Xe^{+2}, Xe^{+3}$.
ΔV = average acceleration voltage = $(f^*_1 \delta V_1 + 2f^*_2 \delta V_2 + 3f^*_3 \delta V_3)/Q$.
$(1-\beta)$ = average voltage utilization efficiency = $\Delta V/V_a$.
β = average fractional loss of acceleration voltage = $1 - \Delta V/V_a$.
χ = Chi Factor = $f_i Q$, charge fraction, moles of charge per mol of propellant.
(1-r) = current utilization efficiency.
r = fractional loss of current, electron recycle fraction.
r_{min} = minimum fraction of current required to ionize propellant.
$\varepsilon_1, \varepsilon_2, \varepsilon_3$ = xenon ionization potentials.
E_1 = first experimental parameter group = $\frac{1}{2}(\mathbf{F}/\dot{m})^2/(V_a \mathscr{F}\mathscr{M}) = \Phi(1-\beta)\chi$.
E_2 = second experimental parameter group = $(\dot{m}/I_a)(\mathscr{F}\mathscr{M}) = (1-r)/\chi$.

I. Introduction

Hall thrusters enable in-space missions that require thousands of hours of thrusting with tens to thousands of mN of thrust.[1] Numerous studies of their performance have appeared in open literature during the last fifteen years. Measurement[2-16] of performance is reported in terms of thrust efficiency (η_{thrust}), defined in terms of measured quantities, $\mathbf{F}$, P_{in} and $\dot{m}$ by:

$$\eta_{thrust} = \frac{1}{2} \frac{\mathbf{F}}{P_{in}} \frac{\mathbf{F}}{\dot{m}}. \qquad (1)$$

In Equation (1) the quantity $\mathbf{F}/P_{in}$ is the thrust to power ratio, an important figure of merit in Hall thruster performance. The second important figure of merit, $\mathbf{F}/\dot{m}$, is the propellant jet specific impulse (impulse per unit mass), which has dimensions of velocity in SI units. Formally, it is the mass weighted average velocity vector of the jet species at the exit surface of the thruster, denoted $\langle \mathbf{v} \rangle$. The term "specific impulse" as commonly used in the

rocket propulsion literature is defined by $I_{sp} = \langle \mathbf{v} \rangle / g_o$, where g_o is the Earth's standard sea-level gravitational constant, $g_o = 9.806$ m/s^2. P_{in} is the anode power, given by $P_{in} = V_a I_a$, where V_a and I_a are the measured quantities. Laboratory measurements are made by setting constant V_a and $\dot{m}$, and then measuring **F** and I_a after tuning the magnetic field strength and topology to minimize I_a (or maximize η_{thrust}). Specific energy investment is defined by $u_{in} = P_{in}/\dot{m}$, which may also be written $u_{in} = \langle \mathbf{v} \rangle / [\mathbf{F}/P_{in}]$. Thus, a standard graph of figures of merit, e.g., thrust to power ratio versus specific impulse, may include lines of constant u_{in} that pass through the chart origin ($\mathbf{F}/P_{in} = \langle \mathbf{v} \rangle / u_{in}$) as well as lines of constant η_{thrust} that may be produced from Eq. (1). Finally, we note that thrust efficiency may be expressed by functions explicit in u_{in}: $\eta_{thrust} = \frac{1}{2} u_{in} (\mathbf{F}/P_{in})^2$, and $\eta_{thrust} = \frac{1}{2} \langle \mathbf{v} \rangle^2 / u_{in}$.

Hall Thrusters have u_{in} values around 100 to 1000 MJ/kg, about 10 to 100 times larger than chemical propulsion systems. Their range of specific impulse may vary by a factor of ten, from ~ 3 to ~ 30 times larger than found in chemical propulsion. Thrust efficiency varies drastically between low and high power Hall thrusters: $\eta_{thrust} < 0.5$ for $P_{in} <$ ~ 600 W, to $\eta_{thrust} \sim 0.7$ for $P_{in} >$ ~ 5 kW. High power thrusters appear to be near their practical upper limit of thrust efficiency. One major determinant of thrust efficiency, the "propellant utilization efficiency", is defined in at least three different ways in the literature, i.e., most commonly as the ionization fraction, but also as the fraction of momentum carried by ions[1], or the beam current charge fraction[2], or the quantity obtained by integrating Faraday probe measurements of beam current around the jet axis at some distance from the exit. In this paper we develop a fundamentally rigorous and simple framework that reconciles various usages of propellant utilization and other utilization efficiencies to enable consistent analysis of various aspects of performance, and, in particular, to enable comparison of performances of low power Hall thrusters to high power Hall thrusters.

II. Velocity Distribution Function

When the velocity distribution function (VDF) of the propellant jet over the exit surface (exhaust) of the thruster is measured, an experimental energy efficiency ($\eta_{energy} = P_{jet}/P_{in}$) may also be extracted from the measured quantities. Since $P_{jet} = \frac{1}{2} \dot{m} \langle \mathbf{v}^2 \rangle$, where $\langle \mathbf{v}^2 \rangle$ is the jet's mass weighted average *squared velocity*, an exact power efficiency equation may be written that applies to any jet, whether continuous or pulsed viz.,

$$\eta_{thrust} = \frac{1}{2} \frac{\mathbf{F}}{P_{in}} \langle \mathbf{v} \rangle = \Phi \frac{P_{jet}}{P_{in}} = \Phi \eta_{energy} , \tag{2}$$

where

$$\Phi = \frac{\langle \mathbf{v} \rangle^2}{\langle \mathbf{v}^2 \rangle} . \tag{3}$$

Equation (2) is an exact mathematical representation, equivalent to $\langle \mathbf{v}^2 \rangle \eta_{thrust} = \langle \mathbf{v} \rangle^2 \eta_{energy}$. It is based on the First Law of Thermodynamics and Newton's Second Law, $P_{jet} = \frac{1}{2} \dot{m} \langle \mathbf{v}^2 \rangle$, and $-\mathbf{F} = d(m\mathbf{v})/dt = \dot{m} \langle \mathbf{v} \rangle$, where $\langle \mathbf{v} \rangle$ is the specific impulse of the propulsive device, i.e., impulse per unit mass or jet velocity. Knowledge of the VDF (i.e., Φ) is necessary and sufficient for calculation of the energy efficiency. For simplicity in the current discussion, the Phi Factor may be factored into two parts, one to represent loss from plume divergence, and one to represent loss from non-uniformity of the VDF that occurs when the jet is composed of species with widely differing velocity.

$$\Phi = \Phi_{div} \Phi_{vdf} . \tag{4}$$

For an isotropic distribution of divergences, with maximum momentum divergence half angle α, Φ_{div} may be expressed by[17]

$$\Phi_{div} = \left(\frac{1 + \cos \alpha}{2} \right)^2 . \tag{5}$$

The quantity within parenthesis is the familiar factor by which thrust of an ideal 1-dimensional rocket jet is reduced due to its 2-dimensional divergence, viz., $\mathbf{F} = \dot{m} \langle v \rangle [(1+\cos \alpha)/2]$

III. Phi Factor for Simple Velocity Distribution Functions

The Φ factor is mathematically limited to $0 < \Phi \leq 1$. For a mono energetic delta function distribution of velocities $\Phi_{vdf} = 1$. For a Maxwellian distribution, $M(\mathbf{v}) = \exp(-\frac{1}{2} m\mathbf{v}^2/kT)$, $\Phi_{vdf} = 8/(3\pi)$. For a Gaussian distribution, $G(\mathbf{v}) = 1/(2\pi\sigma)^{1/2}\exp-[(\mathbf{v}-<\mathbf{v}>)^2/(2\sigma^2)]$, $\Phi_{vdf} = 1/[1 + (\sigma/<\mathbf{v}>)^2]$,[18] where σ is the standard deviation. Chemical rockets produce shifted Maxwellian distributions that are similar to Gaussians with $<\mathbf{v}> \sim 3000$ m/s and $\sigma \sim <$ 10% of $<\mathbf{v}>$, for which $\Phi_{vdf} > 0.99$. Thus, the Φ_{vdf} factor does not often appear in textbook equations where scalar energy quantities are compared to squared vector momentum quantities.

IV. Trimodal Ion Distribution with Neutral Xenon

To show how the Phi Factor depends on the properties of a jet with non-uniform velocity distribution, consider the jet that contains Xe^0, Xe^{+1}, Xe^{+2}, and Xe^{+3} with mass fractions of f_0, f_1, f_2, and f_3, respectively, so that $f_0+f_1+f_2+f_3=1$. To further simplify, we assume the neutral and each ion to have a delta function distribution of velocities, specified by $\mathbf{v}_0$, $\mathbf{v}_1$, $\mathbf{v}_2$, and $\mathbf{v}_3$. This assumption will not significantly affect conclusions that would result from a more complicated model, such as a series of Gaussians for example. In this case the VDF Phi Factor is:

$$\Phi_{vdf} = \frac{\left(\mathbf{v}_o f_o + \mathbf{v}_1 f_1 + \mathbf{v}_2 f_2 + \mathbf{v}_3 f_3\right)^2}{\mathbf{v}_o^2 f_o + \mathbf{v}_1^2 f_1 + \mathbf{v}_2^2 f_2 + \mathbf{v}_3^2 f_3}. \tag{6}$$

For convenience and for compact notation, the ion mass fraction is defined by $f_i = f_1 + f_2 + f_3$, so that $f_0 + f_i = 1$, and reduced ion mass fractions are defined by $f^*_1 = f_1/f_i$, $f^*_2 = f_2/f_i$, and $f^*_3 = f_3/f_i$, so that $f^*_1 + f^*_2 + f^*_3 = 1$. Ratios of velocities of Xe^0, Xe^{+2}, and Xe^{+3} to the velocity of Xe^{+1} are defined by $r_0 = \mathbf{v}_0/\mathbf{v}_1$, $r_2 = \mathbf{v}_2/\mathbf{v}_1$, $r_3 = \mathbf{v}_3/\mathbf{v}_1$. This enables Φ_{vdf} to be written as a function explicit in any two of the three reduced ion fraction variables (f_1^*, f_2*, and f_3^*). In terms of f_1^* and f_2^* the result is:

$$\Phi_{vdf} = f_i \frac{\left[r_0\left(\frac{1-f_i}{f_i}\right) + r_3 + f_1^*\left(1-r_3\right) + f_2^*\left(r_2-r_3\right)\right]^2}{r_0^2\left(\frac{1-f_i}{f_i}\right) + r_3^2 + f_1^*\left(1-r_3^2\right) + f_2^*\left(r_2^2-r_3^2\right)}. \tag{7}$$

First we use Eq. (7) with $f_2^* = f_3^* = 0$ and $r_3 = 0$ to illustrate the dependence of Φ_{vdf} on f_i and r_0 for a two-component jet composed of slow moving neutrals and fast moving, singly charged ions.[1] Figure 1 shows Φ_{vdf} as a function of $\mathbf{v}_1/\mathbf{v}_0$ for this bimodal distribution, with values of f_i from 0.1 to 1 in increments of 0.1. The Figure shows that Φ_{vdf} approaches f_i as $\mathbf{v}_1/\mathbf{v}_0$ approaches infinity; when f_i is larger, as $\mathbf{v}_1/\mathbf{v}_0$ increases, Φ approaches f_i faster. Based on experimental measurements,[12] $\mathbf{v}_0 \sim 200$ m/s, and $\mathbf{v}_1 \sim 20{,}000$ m/s, so $r_0 \sim 0.01$ is appropriate and $\Phi_{vdf} \sim f_i$.

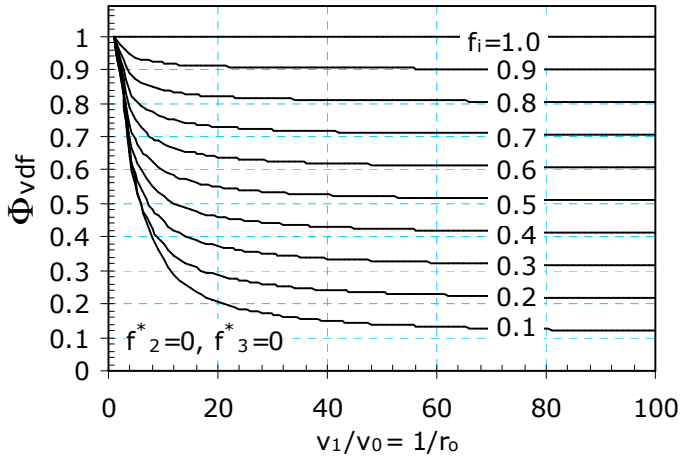

Fig. 1. Dependence of Φ_{vdf} on velocity ratio $\mathbf{v}_1/\mathbf{v}_0 = 1/r_o$ for bimodal velocity distribution with f_i values from 0.1 to 1.0 in increments of 0.1.

Additional thrust inefficiency occurs when the jet is composed of three ion species. This effect may be easily analyzed for an idealization where all three species are created in the same zone whose length is small compared to the acceleration length. In this approximation ion kinetic energies are proportional to their charge so that $r_2 = \mathbf{v}_2/\mathbf{v}_1 = \sqrt{2}$, and $r_3 = \mathbf{v}_3/\mathbf{v}_1 = \sqrt{3}$. Additional approximation is implicit here because ionization potentials are ignored, which is valid so long as they are a small fraction of the acceleration (anode) voltage. Figure 2a shows Φ_{vdf} as a function of $f^*_1$with these velocity ratios for all f^*_1:f^*_2:f^*_3 distributions with f_i values from 0.1 to 1 in increments of 0.1. Figure 2b shows detail of the $f_i = 0.9$ manifold. Experimental findings from RPA and mass spectrometric probes of various thrusters are also plotted in Fig. 2b. Ekholm , et al[15], reported [f^*_1:f^*_2:f^*_3]= [78:15:7], for a relatively highly charged jet (average charge, $Q = f^*_1+2f^*_2+3f^*_3 = 1.29$) of a Busek Hall Thruster (BHT 600) running under optimum conditions with P_{in} = 600 W, V_a = 300V, $\dot{m}$ = 2.5 mg/s, $\eta_{thrust} = 0.555$.[14] Hofer, et al.[4,5] studied several NASA Hall Thrusters. For the 173Mv2 thruster, they reported variation of [f^*_1:f^*_2:f^*_3] from [96:3:1], Q = 1.05, to [81:16:3], Q = 1.22 as V_a increased from 300 to 900 volts, and specific impulse increased from ~ 10 to 30 km/s. Gulzcinski, et al.[10] made mass spectrometric measurements in the near and far field of plumes of the P5 Hall thruster and reported large decreases in average charge as distance from the exit increased; their measurement for the distribution with largest Q is indicated in Fig. 2b. The departure of Φ_{vdf} from f_i at $f_i = 0.9$ is less than 1% to 2% for Hofer distributions and ~ 3.5% for the Ekholm and Gulczinski distributions.

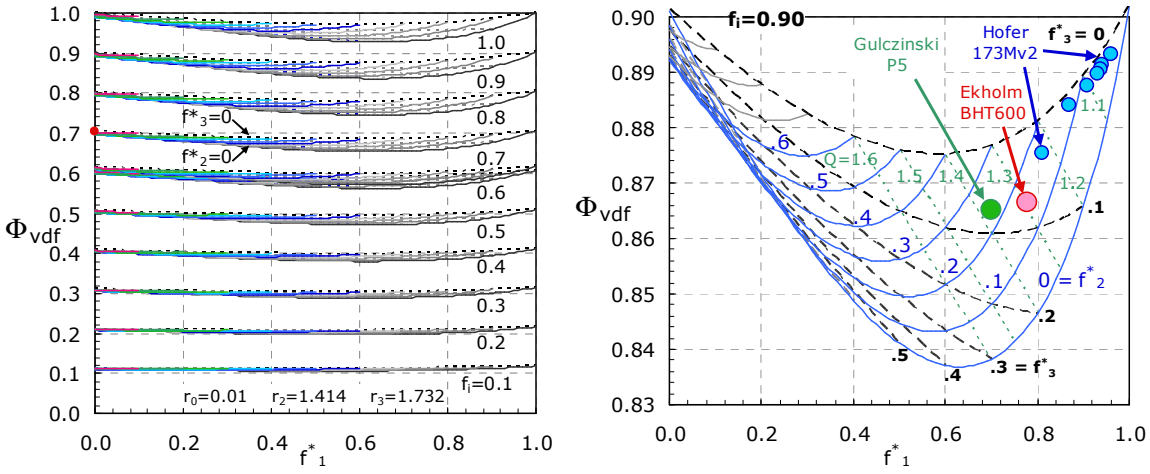

Fig. 2. (a) VDF Phi Factor for jet composed of neutrals and three ions. Ten manifolds of f^*_1, f^*_2, f^*_3 distributions are shown at f_i values from 0.1 to 1 at f_i increments of 0.1.
(b) Detail of Φ_{vdf} for f_i = 0.9 manifold showing lines of **constant f^*_2 (blue solid lines)**and **constant f^*_3 (black dashed lines)** from 0 to 1 and lines of **constant Q (green dotted lines)** from 1.1 to 1.6. The locations of points for the Ekholm distribution, several Hofer distributions (where Φ_{vdf} decreases with increasing Q and V_a), and the Gulczinski distribution are also shown.

Figure 3 shows the deviation of Φ_{vdf} from the $\Phi_{vdf} = f_i$ approximation as a graph of [$\Phi_{vdf} - f_i$] vs f_i. Eq. (7) may be used to show that the envelope of all deviations is bounded by the hypothetical distributions [f^*_1:f^*_2:f^*_3] = 100:0:0 (Q = 1) and [60:0:40] (Q = 1.8), which is apparent from the minimum Φ_{vdf} shown in Fig. 2b. Fig. 3 shows that [$\Phi_{vdf} - f_i$] may be expressed by a linear function of f_i over a large range of f_i and that the effect of VDF non-uniformity may be approximated with a simple relationship: $\Phi_{vdf} \approx af_i$. Table 1 summarizes details for these distributions and establishes a highly correlated linear relation between Q and a, i.e., Q = 9.6-8.6a.

Table 1. Summary of ion distributions in three Hall thrusters: Q = 9.6-8.6a.

distribution	f_1^*:f_2^*:f_3^*	Q	a = Φ_{vdf}/f_i from Eq. (7) with f_i = 0.9
limit	100:00:00	1.00	1.000
Hofer 173Mv2	96:03:01	1.05	0.993
Hofer 173Mv2	93:06:01	1.08	0.989
Hofer 173Mv2	87:12:01	1.14	0.982
Hofer 173Mv2	81:16:03	1.22	0.973
Ekholm BHT 600	78:15:07	1.29	0.963
Gulczinski P5	70:23:07	1.37	0.961

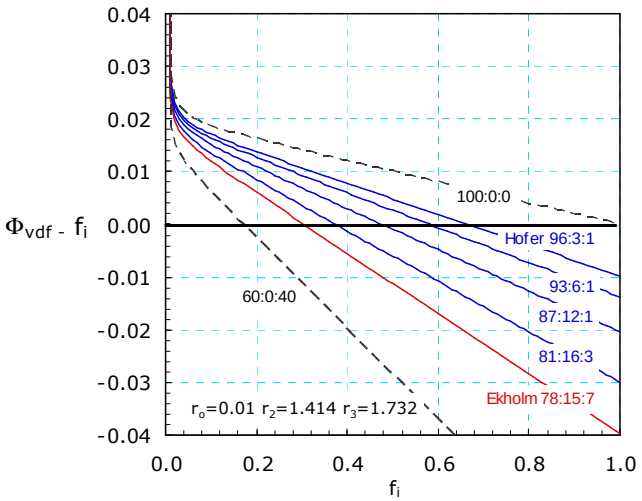

Fig. 3. $[\Phi_{vdf} - f_i]$ vs f_i. Departure of Phi Factor from $\Phi_{vdf} = f_i$ approximation as a function of f_i for hypothetical distributions and Ekholm, and Hofer distributions.

V. Propellant, Voltage, and Current Utilization Efficiencies

Equation (1), may be written in a form that reveals thrust efficiency to be a product of three separate efficiency terms, viz.,

$$\eta_{thrust} = \frac{\left(\frac{\mathbf{F}}{\dot{m}}\right)^2}{<\mathbf{v}^2>} * \frac{<\mathbf{v}^2>}{<\mathbf{v}^2>_+} \frac{\frac{1}{2}<\mathbf{v}^2>_+}{\frac{\mathcal{F}}{\mathcal{M}} V_a} * \frac{\dot{m}}{I_a} \frac{\mathcal{F}}{\mathcal{M}}. \tag{8}$$

The first term in Eq. (8) is the Φ-factor, which is defined by Eqs. (2-3). As used in this paper, the Φ-factor has attributes of a good "propellant utilization efficiency." As Eq. (3) shows, it is always less than unity and it approaches unity as propellant utilization approaches perfection. It captures the loss of propellant utilization in three ways: (1) by quantifying loss of utilization due to incomplete ionization, (2) by quantifying loss of thrust due to distribution of energy among several ion species as in Eqs. (6-7), and (3) by quantifying loss of thrust due to divergence of the propellant trajectory from the thrust axis as in Eqs. (4-5). The Φ-factor is unity for a perfect, mono-energetic jet with one ion species, no neutral atoms, and no divergence. Also, as shown by Fig. 3, Φ_{vdf} is only slightly less than the ionization fraction. Several usages of the term "propellant utilization" have appeared in the literature, ranging from the review of Zhurin et al.,[1] where it is the fraction of momentum carried by ions, to the paper by Raitses, et al.[2] where it is the ratio of beam current to mass flow, to frequent usages where it is simply referred to as the ionization fraction.

The second term of Eq. (8) may be transformed into an expression that contains explicit voltage utilization efficiencies for each ion species, $\delta V_1/V_a$, $\delta V_1/V_a$, $\delta V_1/V_a$, such as may be directly measured with an ExB probe. Also, an expression may be derived that defines an average voltage utilization efficiency, $\Delta V/V_a$, such as may be directly measured with a retarding potential analyzer, RPA. First, one may obtain the leading ratio of the second term of Eq. (8), $<\mathbf{v}^2>/<\mathbf{v}^2>_+$, as follows:

$$\frac{<\mathbf{v}^2>}{<\mathbf{v}^2>_+} = \frac{f_0\mathbf{v}_0^2 + f_1\mathbf{v}_1^2 + f_2\mathbf{v}_2^2 + f_3\mathbf{v}_3^2}{f_1^*\mathbf{v}_1^2 + f_2^*\mathbf{v}_2^2 + f_3^*\mathbf{v}_3^2} = f_i\left[1 + \frac{r_0^2\left(\frac{1-f_i}{f_i}\right)}{f_1^* + f_2^* r_2^2 + f_3^* r_3^2}\right] \approx f_i \tag{9}$$

It may be shown that the bracketed quantity of Eq. (9) is very close to unity under all reasonable conditions of operation of a Hall thruster because the term in numerator of the quotient is very small, i.e., $r_0^2(1-f_i)/f_i \sim 1x10^{-5}$,

compared to the denominator. Thus, the approximation, $\langle \mathbf{v}^2 \rangle / \langle \mathbf{v}^2 \rangle_+ \approx f_i$ is accurate to better than ten parts per million.

The kinetic energy of an ion species is proportional to the product of its charge, z, and acceleration voltage, δV, e.g., $\frac{1}{2}\mathbf{v}^2 = z\delta V \mathcal{F}/\mathcal{M}$, so the average specific ion energy may be written for a propellant jet composed of three ion species:

$$\frac{1}{2} < \mathbf{v}^2 >_+ = \frac{\mathcal{F}}{\mathcal{M}} \left(f_1^* \delta V_1 + 2 f_2^* \delta V_2 + 3 f_3^* \delta V_3 \right), \tag{10}$$

where δV_1, δV_2, and δV_3, are the voltages through which the three ions are accelerated. Using Eq. (9) and (10), one may write the second term of Eq. (8) as follows:

$$\frac{< \mathbf{v}^2 >}{< \mathbf{v}^2 >_+} \frac{\frac{1}{2} < \mathbf{v}^2 >_+}{\frac{\mathcal{F}}{\mathcal{M}} V_a} = f_i \left[f_1^* \frac{\delta V_1}{V_a} + 2 f_2^* \frac{\delta V_2}{V_a} + 3 f_3^* \frac{\delta V_3}{V_a} \right] \tag{11}$$

An average voltage utilization efficiency, $\Delta V / V_a = (1-\beta)$, may be defined so as to make use of measurement of kinetic energy (voltage) per unit charge with an RPA. Thus,

$$f_i \left[f_1^* \frac{\delta V_1}{V_a} + 2 f_2^* \frac{\delta V_2}{V_a} + 3 f_3^* \frac{\delta V_3}{V_a} \right] = f_i \frac{\Delta V}{V_a} \left(f_1^* + 2 f_2^* + 3 f_3^* \right) = (1-\beta) f_i Q \tag{12}$$

In Eq. (12) the average charge is defined by $Q = f_1^* + 2f_2^* + 3f_3^*$. Average acceleration voltage is defined by $\Delta V = [f_1^* \delta V_1 + 2 f_2^* \delta V_2 + 3 f_3^* \delta V_3]/Q$. The β quantity is the average fractional acceleration voltage loss, so that $(1-\beta) = \Delta V / V_a$ is the average voltage utilization efficiency.

Another useful property of the jet that appears in Eq. (12) is denoted the Chi-factor, $\chi = f_i Q$, which is similar to the Φ-factor because they are both proportional to f_i. Although the χ-factor contains information about ionization fraction, it is not suitable as a utilization efficiency because it may have a value greater than unity, e.g., in highly ionized plasmas with highly charged ions. The quantity $[\chi \dot{m} \mathcal{F}/\mathcal{M}]$ is the total positive ion current exiting the thruster, frequently called the beam current, which is the quantity obtained in a good Faraday probe measurement. χ may also be thought of as the positive charge fraction, or as the moles of positive charge flow per mole of propellant flow.

The third term of Eq. (8) may be transformed into the quotient of a current utilization efficiency, (1-r), and the χ-factor, viz.,

$$\frac{\dot{m}}{I_a} \frac{\mathcal{F}}{\mathcal{M}} = \frac{(1-r)}{\chi}, \tag{13}$$

by transforming the equation of mass and charge conservation, viz.,

$$(1-r) I_a = \dot{m} \frac{\mathcal{F}}{\mathcal{M}} \chi = \dot{m} \frac{\mathcal{F}}{\mathcal{M}} f_i \left(f_1^* + 2 f_2^* + 3 f_3^* \right). \tag{14}$$

In Eqs. (13) and (14), r is the "electron recycle fraction", the fraction of electrons that recycle from the cathode, through the acceleration channel, and to the anode. Recycled electrons ionize neutral propellant and sustain dissipative plasma processes. Energy not used for ionization is lost by joule heating; the total power loss is $r I_a V_a$. The $r I_a$ quantity may be thought of as the Hall current required to sustain plasma ionization. The quantity $(1-r) I_a$ represents the beam current, which is the electron current utilized in neutralization of the positive charge flow leaving the thruster. The minimum electron recycle fraction, r_{min}, is the fraction of the anode current, Ia, that carries the amount of power necessary to produce a given ionization fraction of specified ion distribution, which is given by:

$$r_{min} = \frac{\dot{m}}{I_a V_a} f_i \left(\varepsilon_1 f_1^* + \varepsilon_2 f_2^* + \varepsilon_3 f_3^* \right) \tag{15}$$

where ε_1, ε_2, and ε_3 are the first, second and third ionization potentials of xenon. Eq. (15) may also be written as $r_{min} = u_{ion}/u_{in}$, where $u_{ion} = f_i(\varepsilon_1 f_1^* + \varepsilon_2 f_2^* + \varepsilon_3 f_3^*)$ is the specific energy required to produce ion fraction f_i with specified species distribution $[f_1^*:f_2^*:f_3^*]$.

Substitution of the mass, energy and charge conservation principles embodied in Eqs. (9)-(14) into Eq. (8) allows thrust efficiency to be written as a product of three utilization efficiencies, viz.,

$$\eta_{thrust} = \Phi(1-\beta)\chi * \frac{(1-r)}{\chi} = \Phi(1-\beta)(1-r), \tag{16}$$

and the energy efficiency to be written as a product of voltage and current utilization efficiencies, independent of, and rigorously separable from, propellant utilization efficiency, viz.,

$$\eta_{energy} = (1-\beta)(1-r). \tag{17}$$

The recent paper by Hofer and Gallimore[11] presents a comprehensive study of the performance of the NASA 173Mv2 Hall thruster and sets forth an approach for efficiency analysis that includes definitions of voltage utilization efficiency (1-β) and current utilization efficiency (1-r) that are identical to the definitions used here. However, in their system, anode thrust efficiency, defined as in Eq. (1) of this paper, is the product of four utilization efficiencies, (1-β), (1-r), and two other utilization efficiencies, termed mass utilization efficiency, η_m, and charge utilization efficiency, η_q. The product of their mass and charge utilization efficiency, $\eta_q\eta_m$, is almost exactly equivalent to our Φ_{vdf} as defined by Eq. (7), and as approximated by $\Phi_{vdf} = af_i$, where f_i represents the *quantity* of propellant utilization and a represents the *quality* of propellant utilization. The Hofer-Gallimore η_m is identical to f_i, and their η_q is nearly identical to our a, except that their η_q does not include the terms involving neutral xenon, i.e., terms involving r_o in Eq.(7). But, this difference makes their $\eta_q \sim 0.2\%$ smaller than our a when $f_i > 0.9$. Further, the difference between a and η_q disappears entirely when the propellant ionization fraction reaches unity.

The Hofer-Gallimore expression for anode thrust efficiency does not include a term for loss of thrust due to momentum divergence of the propellant jet. Eq. (5) shows that the divergence loss factor may be significant. When the momentum divergence half angle increases from α = 20-to 30-degrees, Φ_{div} decreases from 0.94 to 0.87. Thus, the ionization fraction (f_i) achieved by the 173Mv2 that was reported as 0.87 will be significantly larger when divergence loss is accounted for, i.e., f_i = 0.93 if α = 20-degrees, or f_i = 1.0 if α = 30-degrees. Also, since the ionization fraction must be less than unity, α must be less than 30-degrees.

VI. Extraction of Utilization Efficiencies from Experimental Quantities

Two quantities, E_1 and E_2, that mix the utilization efficiencies with the χ-factor may be obtained directly from groups of experimentally measured quantities.

$$E_1 = \Phi(1-\beta)\chi = \Phi_{div} a Q (1-\beta) f_i^2 = \frac{\frac{1}{2}\left[\frac{\mathbf{F}}{\dot{m}}\right]^2}{V_a \frac{\mathcal{F}}{\mathcal{M}}}, \tag{18}$$

and

$$E_2 = \frac{(1-r)}{\chi} = \frac{(1-r)}{f_i Q} = \frac{\dot{m}}{I_a}\frac{\mathcal{F}}{\mathcal{M}}. \tag{19}$$

Thrust efficiency then may then be expressed simply: $\eta_{thrust} = E_1 E_2$. Thus, graphs of E_1 vs E_2 with lines of constant η_{thrust} may be prepared to enhance insightful analysis. For example, as f_i increases while other parameters [Φ_{div}, a, Q, r, and β] are constant, E_1 increases proportional to the square of f_i and E_2 decreases proportional to the reciprocal of f_i.

Experimental studies that include measurement of beam current [beam current = $(1\text{-}r)I_a$] with use of Faraday probe scans of the plume around the thrust axis and at some distance away from the thruster exit enable extraction of additional performance data because χ may be obtained by Eq. (14). Then current utilization efficiency, (1-r) may be obtained directly from Eq. (19), and the product of propellant utilization efficiency and voltage utilization efficiency, $\Phi(1\text{-}\beta)$, may be obtained directly from Eq. (18). Further deconvolution may be accomplished by using the previously discussed relationship between Q and a ($Q = 9.6 - 8.6a$), which enables setting limits on permissible values of fi, Q, and the geometric mean of the momentum divergence phi factor and voltage utilization efficiency, $[\Phi_{div}(1\text{-}\beta)]^{1/2}$. Since $fi = \chi/Q$ and

$$f_i\sqrt{\Phi_{div}(1-\beta)} = \sqrt{\frac{E_1}{Qa}} = \sqrt{\left(\frac{E_1}{Q}\right)\left(\frac{8.6}{9.6-Q}\right)}, \tag{20}$$

a graph of f_i vs $[\Phi_{div}(1\text{-}\beta)]^{1/2}$ may be produced that shows permissible solutions that depend on E_1 and Q.

Direct measurement of voltage utilization efficiency, $(1\text{-}\beta)$, may be accomplished with use of a retarding potential analyzer, and performance may be further specified by an expression of f_i as a function of Φ_{div}. Finally, if the VDF is determined with an ExB probe or by LIF, a complete set of performance parameters, Q, f_i, Φ_{div} and $(1\text{-}\beta)$ may be deduced.

VII. Applications to Hall Thrusters - Cylindrical Hall Thruster

There is extensive literature on Hall thruster performance. Here we analyze several sets of notable data[2-16] to illustrate the distinctions between thrust and energy efficiency and the expression of thrust efficiency as a product of the three utilization efficiencies. First, we examine the performance of a Cylindrical Hall Thruster (CHT) reported by Raitses, et al.[2]. Five CHTs with various channel geometries were operated at powers up to ~ 600 W. Systematic measurement of $\mathbf{F}$, $\dot{m}$, I_a, V_a, and χ (with Faraday probe) were reported. Results from all the geometries were transcribed from the graphical presentations in the published paper and tabulated in Table 1 of the Appendix to this paper, along with calculated values of η_{thrust}, $\mathbf{F}/P_{in}$, $\langle \mathbf{v} \rangle$, $\Phi(1-\beta)\chi$, and $(1-r)/\chi$. Also, since χ was measured, values of the current utilization efficiency (1-r) and the product of propellant and voltage utilization efficiency, $\Phi(1-\beta)$, could be extracted. Other relationships between Φ_{div}, f_i, Q and their limits are also derived from the data..

Here, we analyze the optimum CHT geometry, which had a 30-mm acceleration channel with 10-cm^2 cross section. Figure 4 shows two performance runs at each of three anode voltages, 200 V, 250 V, and 300 V. Each run consisted of a thrust measurement at each of six flow rates. After setting V_a and $\dot{m}$, the magnetic fields were adjusted to minimize I_a. Then I_a and $\mathbf{F}$ were recorded. At the same time the total positive ion beam current was measured with a Faraday probe, and this enabled determination of χ. The χ-factor is moles of positive charge per mole of propellant, and may be thought of as a molar charge fraction as defined in Eq. (14).

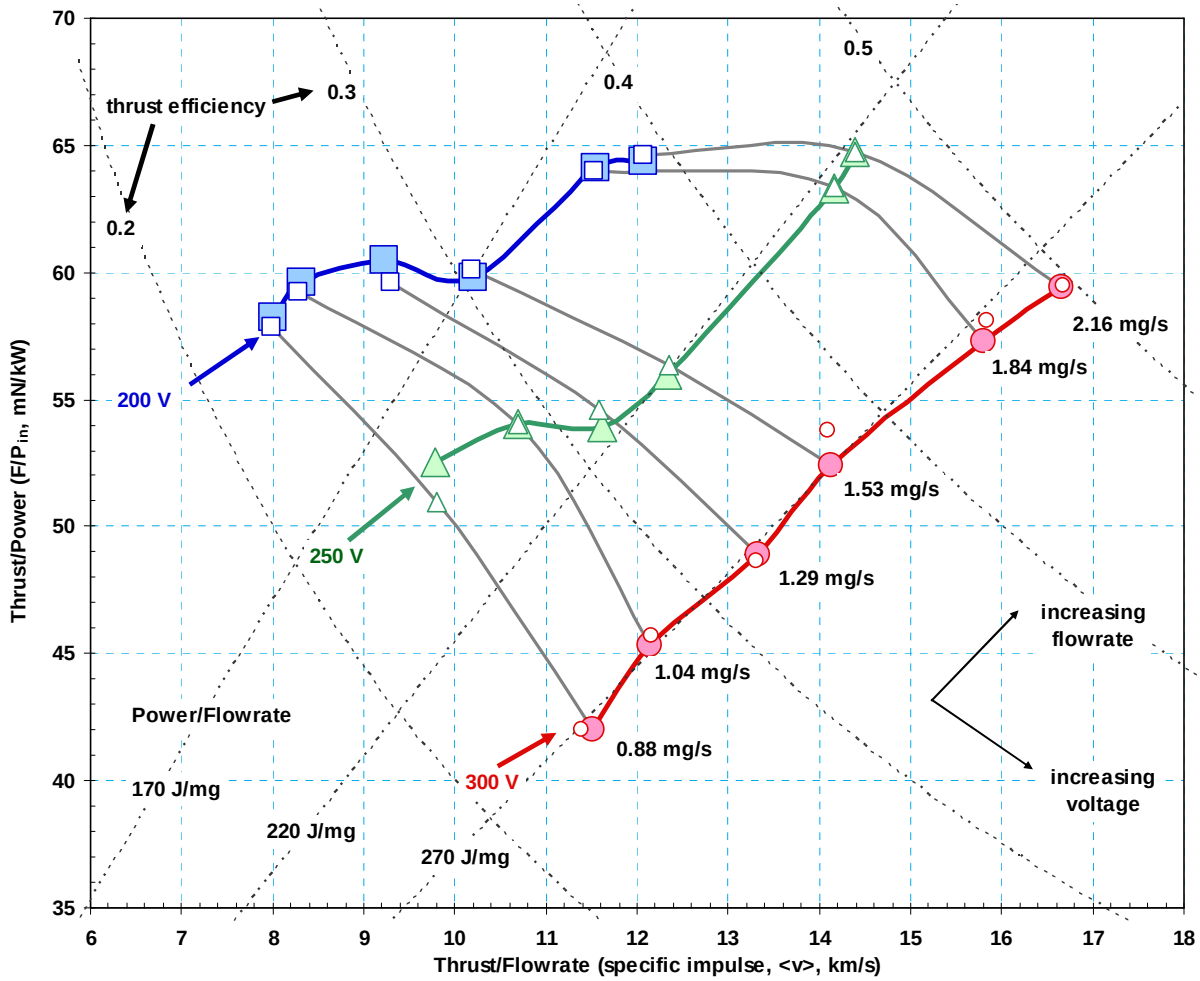

Fig. 4. Performance of the optimum CHT geometry (30 mm acceleration channel with 10 cm^2 cross section) calculated from the data reported by Raitses, et al.[2]. Two series of data were acquired at each voltage: V_a = 200 V (squares), 250 V (triangles), and 300 V (circles). Data points at 6 mass flow rates, (0.88, 1.04, 1.29, 1.53, 1.84, 2.16 mg/s) show increasing efficiency with increasing mass flow rate. Lines of constant thrust efficiency (η_{thrust} = 0.2, 0.3, 0.4, and 0.5) and lines of constant specific input energy (u_{in} = 170-, 220-, and 270-J/mg) are shown. Note that $u_{in} = V_a(\mathscr{F}\!/\mathscr{M})\chi/(1-r)$. At 300 V, the figure shows that $\mathbf{F}/P$ vs $\langle \mathbf{v} \rangle$ approximately tracks the constant u_{in} = 270 J/mg line; thus, at 300 V, when flow rate increases, $\chi/(1-r)$ remains constant.

Figure 5 shows the E_2 vs E_1 graph and the χ-factor (f_iQ) vs I_a graph as obtained from experimental data. The left graph shows E_1 vs E_2 with lines of constant η_{thrust}, which is based only on the $\mathbf{F}, \dot{m}$, I_a, V_a data. The abscissa, E_1, is proportional to the square of the ion mass fraction, f_i^2, i.e., $E_1 = \Phi(1-\beta)\chi = \Phi_{div}af_i(1-\beta)f_iQ$. The ordinate, E_2, is proportional to the reciprocal of f_i, i.e., $E_2 = (1-r)/\chi = (1-r)/f_iQ$. Thus, the pathway of increasing f_i at constant r, β, a, Q, and Φ_{div} is downward to the right, as shown in the left graph. The Figure shows that the lower flow rate data at V_a = 200 V and 250 V follow lines of increasing f_i and level off, coincident with V_a = 300 V, at (1-r)/χ ~ 0.8. The χ vs discharge current graph on the right side of Fig. 5 is obtained from the beam current as measured with a Faraday probe, i.e., beam current = $(1-r)I_a = \dot{m}\chi(\mathcal{F/M})$.

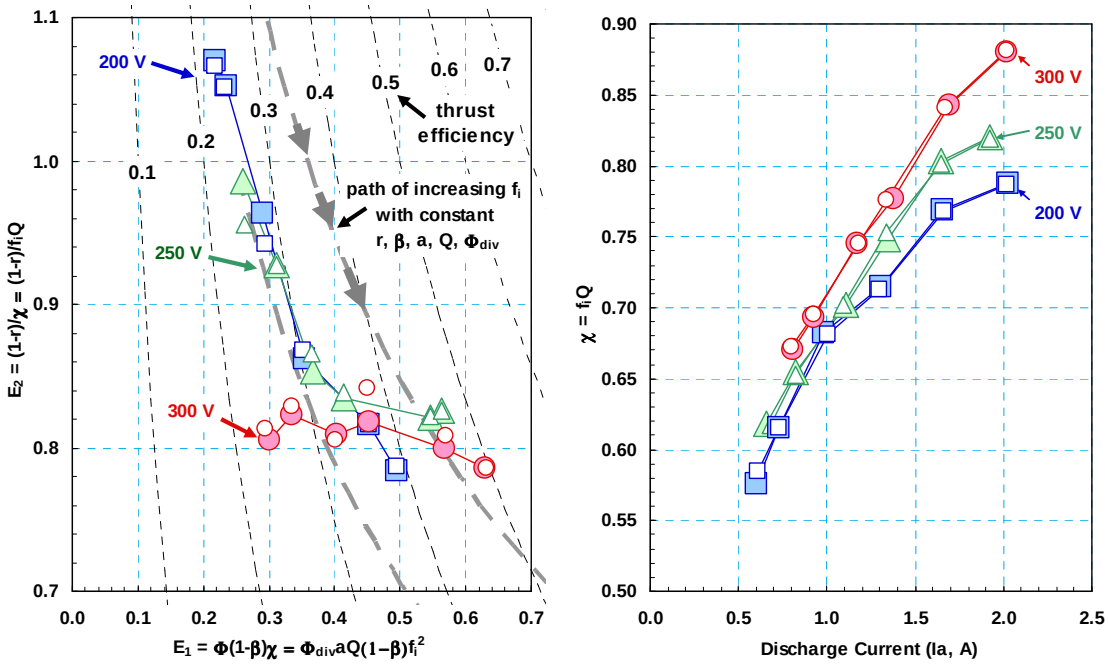

Fig 5. Performance of the optimum geometry of the Cylindrical Hall Thruster (CHT, L = 30 mm, A = 10 cm^2) calculated from data of Raitses, Ashkenazy, and Guelman.[2] Graph of Chi factor vs discharge current was obtained from measurement of beam current by integration of Faraday probe data.

As shown in Fig. 6, use of the χ-factor with Eqs. (18) and (19) enables construction the graph of (1-r) vs $\Phi(1-\beta)$. At the optimum operating point the measured quantities were V_a = 300 V, $\dot{m}$ = 2.16 mg/s, I_a = 2.02 A, **F** = 36.0 mN, and χ = 0.881, which enabled calculation of η_{thrust} = 0.496, E_1 = 0.631, E_2 = 0.786, (1-r) = 0.692, and $\Phi(1-\beta)$ = 0.716, see appendix. Making use of the relationship between Q and a (Table 1) and the definitions $\Phi_{vdf} = af_i$ and $\chi = f_iQ$, and Eq. (18), one may derive a relation to enable consistent sets of values of Q, (1-β), Φ_{div}, and f_i to be determined.

Equation (20) was used to produce Figure 7, which shows a plot of the geometric mean of the divergence part of propellant utilization efficiency, Φ_{div}, and the voltage utilization efficiency (1-β) as a function of f_i for each of the six flow rates at each of the three voltages and over a range of average ion charge, Q from 1.0 to ~ 1.35.. The figure shows the restrictions on the parameters that are imposed by the data and by the requirements that $Q \geq 1$, and $[\Phi_{div}(1-\beta)]^{1/2} \leq 1$. Several conclusions may be drawn from Fig. 7. For example, at anode voltage of 300V and flow rate of 2.16 mg/s, the value of f_i must lie between ~ 0.88 (where Q = 1, $[\Phi_{div}(1-\beta)]^{1/2}$ =~ 0.9) and ~ 0.73 (where Q = 1.2, $[\Phi_{div}(1-\beta)]^{1/2}$ ~ 1). If Q remains constant at Q = 1.1 during the increase of flow rate from 0.88 to 2.16 mg/s, f_i must increase from ~ 0.60 to 0.80 and $[\Phi_{div}(1-\beta)]^{1/2}$ must increase from 0.86 to 0.95. If $[\Phi_{div}(1-\beta)]^{1/2}$ remains constant at 0.90 during the increase of the flow, f_i must increase from 0.56 to 0.88 and Q *must decrease* from ~ 1.18 to 1.0. Also, at the highest flow, a value of Q = 1.1 is consistent with f_i = 0.8, (1-β) = .95, and Φ_{div} = 0.95 (or α = 18-degrees). The extreme values of Q = 1, f_i = 0.88, $(1-\beta)_{max}$ = 0.965 that apply to perfect ionization (i.e., f_i = 0.88, f_1^* = 1, single Xe^{+1}ion) and perfect voltage utilization are consistent with a value of the maximum permissible momentum divergence loss, Φ_{div} = 0.84, or α = 34-degrees. Similar conclusions may be extracted for the lower anode voltage operations.

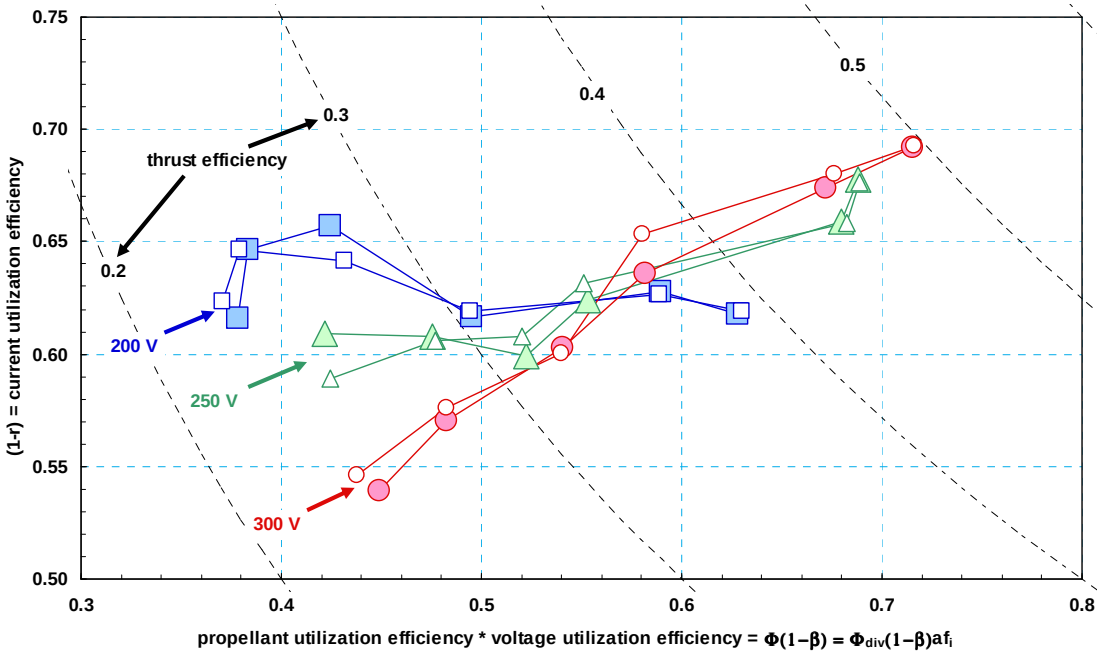

Fig 6. Performance of Cylindrical Hall Thruster (CHT) optimum geometry: L = 30 mm, A = 10 cm^2 calculated from data of Raitses, Ashkenazy, and Guelman.[2]

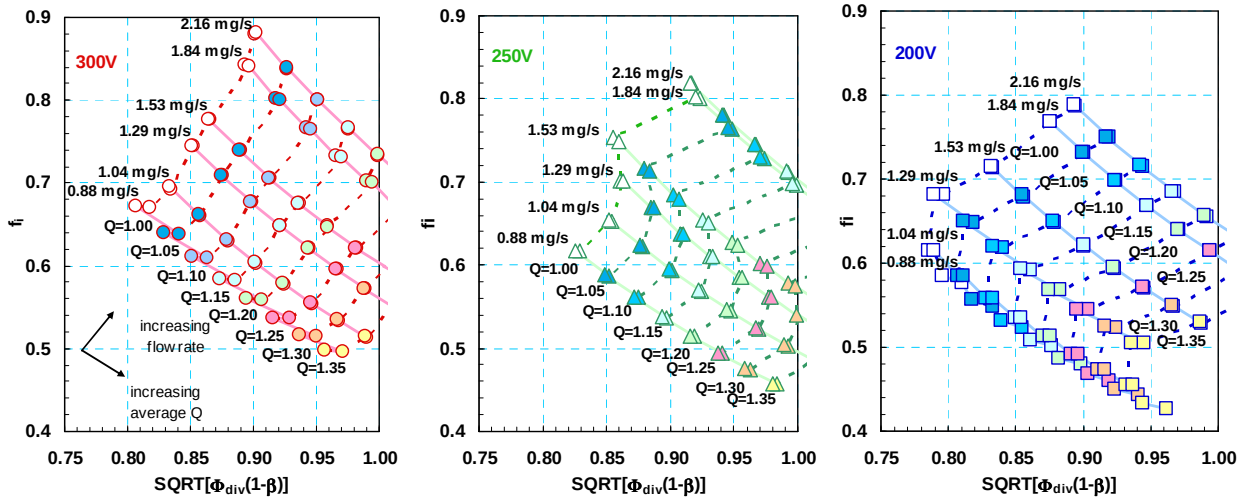

Fig. 7. Parameter Consistency diagrams for CHT optimum geometry: L = 30 mm, A = 10 cm^2. The diagrams show values of f_i, $[\Phi div(1-\beta)]^{1/2}$, and Q that are consistent with each other at each of the six experimental flow rates and each of the three anode voltages: Va = 300 V (left), 250 V (center), and 200 V (right).

VIII. Applications to Hall Thrusters – Comparison of High and Low Power Thrusters

Figure 8 shows a summary of experimental performance data (thrust vs specific impulse with lines of constant anode power, and lines of constant flow rate) for Hall thrusters ranging from ~ 200 Watts to ~ 50 kilowatts and specific impulse ranging from ~ 1000 seconds to 5000 seconds. The Figure includes data for the optimum CHT geometry operated at three anode voltages (V_a = 200, 250, and 300 V)[2]. Data from the SP30[6] and the SP50[9], operated between V_a = 200 and 400 V and the BHT-200-X2B[7] operated at V_a = 300 V are also shown. Also included are data from higher power thrusters, P5[4], 173Mv1[4], 173Mv2[4], 173Mv1A2[4], as well as data from 173Mv1 with Krypton[3], and data from the SP400 with krypton and xenon[15]. Optimum operating points for three Busek Hall Thrusters of (600 W[14], 8 kW[16], and 20 kW[16]) are shown. Anode voltages for the SP400 with xenon, V_a = 200, 300, 400, 500, and 600 V are indicated on the figure to show the systematic increase of specific impulse with the square root of V_a. This approximate dependence of <v> on V_a is apparent in all Hall thruster data.

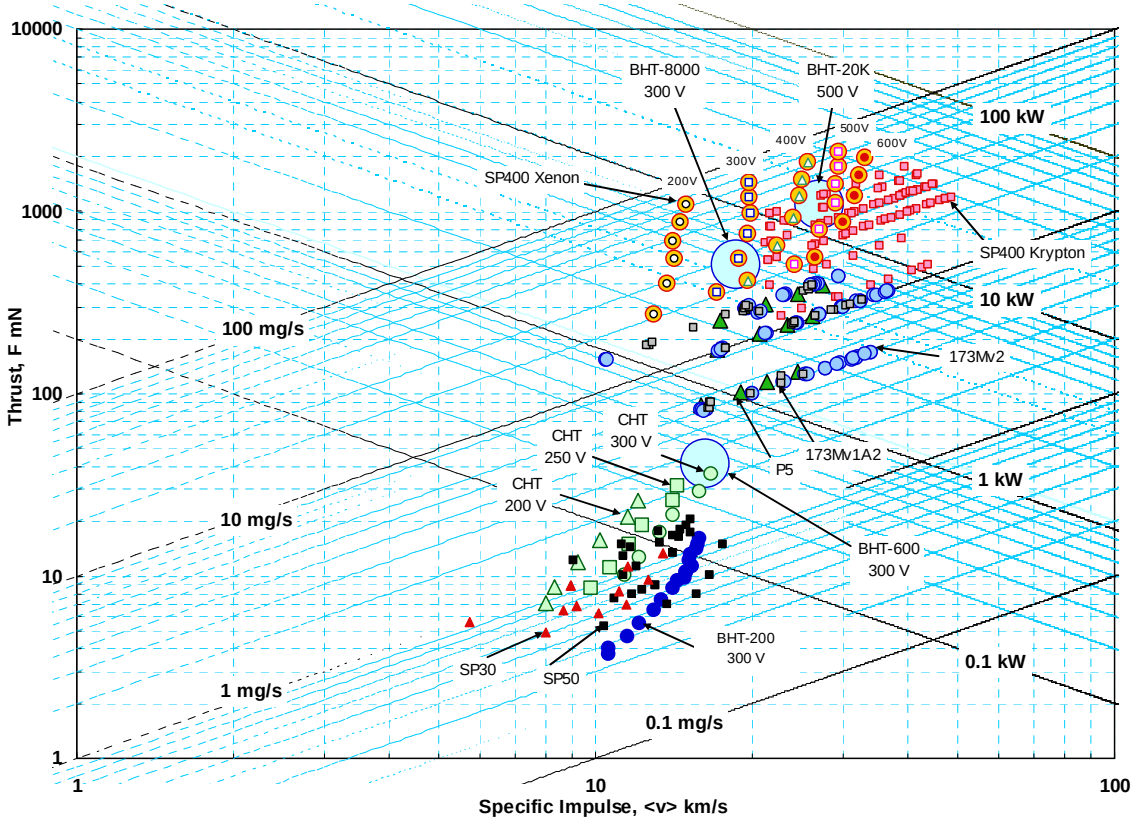

Fig. 8. Thrust vs specific impulse for several Hall thrusters showing lines of constant jet thrust power (i.e., jet thrust power = $[\mathbf{F}^2/(2\dot{m})]$ = 0.1, 1, 10, 100-kW), and lines of constant propellant flow rate (0.1, 1, 10, 100-mg/s). Data from Refs 2-=16.

Addition of the experimental data on input power to the data of Figure 8 produced Figure 9, which is a primary performance map showing the thrust to power ratio as a function of specific impulse. Figure 10 shows the E_1 vs E_2 plot, $E_1 = \Phi(1-\beta)\chi = \Phi_{div}aQ(1-\beta)f_i^2$, and $E_2 = \Phi(1-r)/\chi = (1-r)/f_iQ$. Fig. 10 shows that the pathways of increasing f_i (at constant r, β, Q, a, and Φ_{idv}) cuts across lines of constant η_{thrust}, downward and to the right, which is also the direction of increasing V_a and $\dot{m}$.

Figure 10 shows for the high power thrusters that higher anode voltage produced higher η_{thrust}, which was accompanied by smaller $(1-r)/\chi$ in all the thrusters. It is interesting that $E_1 = \Phi_{div}aQ(1-\beta)f_i^2 > 1$ is produced in SP 400 with xenon at anode voltages V_a > 400 V. The average charge is the only factor in E_1 that may exceed unity, so E_1 is the lower limit of Q under these operating conditions of SP 400..

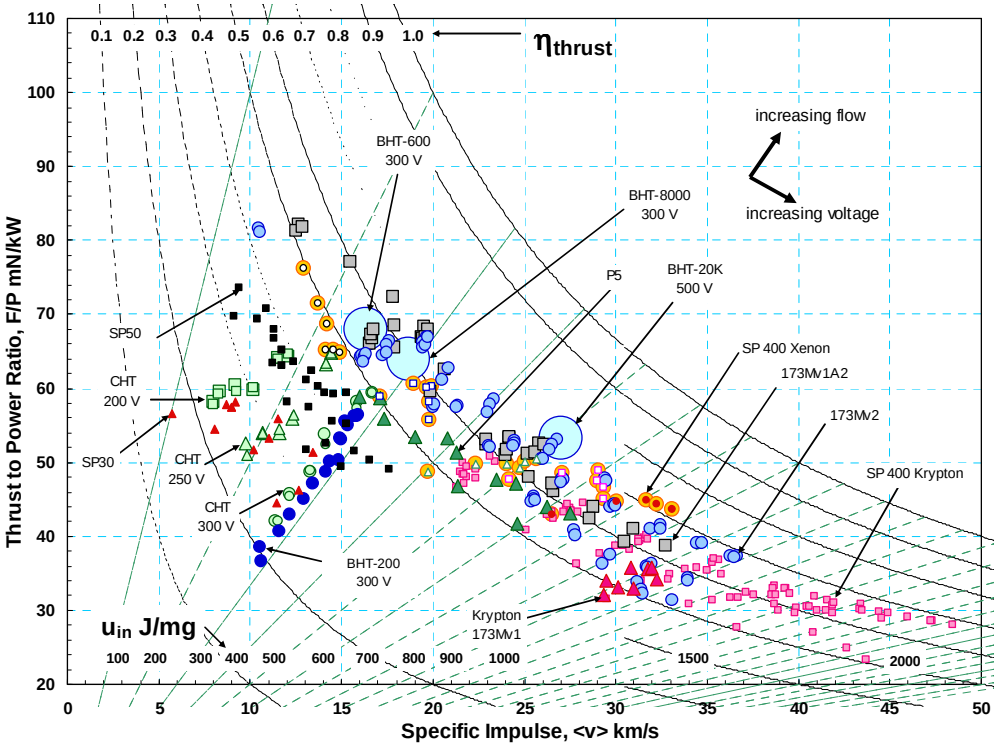

Fig.9. Performance of several Hall thrusters with range of input power from 200 W to 50 kW showing lines of constant thrust efficiency and lines of constant specific internal energy input. Data from Refs. 2-16

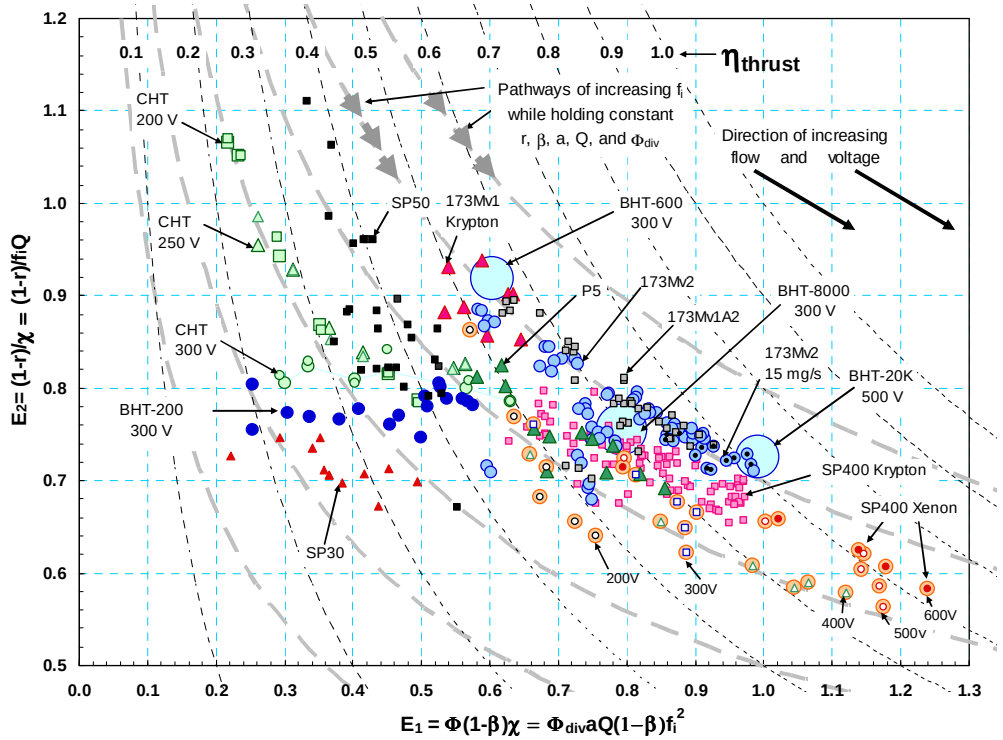

Fig. 10. Performance of Hall thrusters with range of input powers from 200 W to 50 kW with lines of constant thrust efficiency. Abscissa, E_1, is proportional to the square of ion mass fraction. The direction of pathways of increasing f_i (at constant r, β, a, Q, and Φ_{div}) are shown cutting across lines of constant η_{thrust}, approximately tracking the data in the direction of increasing flow and/or anode voltage. Data from Refs. 2-16.

IX. Summary

A rocket power efficiency equation was derived to explicitly account for the effect of the velocity distribution function (VDF) of the propellant jet on the conversion of anode electrical energy to jet kinetic energy. This enabled a mathematically rigorous distinction to be made between thrust efficiency and energy efficiency. In this approach, thrust efficiency, the commonly reported figure of merit for Hall thrusters, is the product of three utilization efficiencies: (1) propellant utilization efficiency, (2) voltage utilization efficiency, and (3) current utilization efficiency. The three utilization efficiencies are well behaved, being less than unity under all real operating conditions and approaching unity as energy conversion approaches ideality. Perfect propellant utilization is characterized by 100 percent ionization to a single ionic species whose thrust vectors are all directed along the same thrust axis. Anode voltage utilization efficiency is unity when ion species are created at the anode and accelerated through the entire anode potential. Current utilization efficiency is the fraction of cathode electron flow utilized in neutralization of accelerated positive ions. It can never be unity because a portion of the electron flow must be recycled back to the anode to provide energy to ionize neutral propellant. The architecture of the efficiency analysis is such that energy efficiency becomes naturally expressed as a product of voltage and current utilization efficiencies. Energy efficiency is rigorously separated from propellant utilization efficiency. Thus, thrust efficiency is the product of propellant utilization efficiency and energy efficiency. The methodology developed was applied to analysis of data from systematic studies of performance of low and high power Hall thrusters.

Numerous Hall thruster performance studies have been published in the open literature. The basic data set (measurements of thrust, propellant mass flow rate, anode voltage, and anode current) are frequently coupled with measurement of plasma plume properties using other optical or electrical diagnostics. Data that enables calculation of propellant utilization, Φ, and average charge Q may be obtained with an ExB probe, by Laser Induced Fluorescence, or with use of mass spectrometry. A Retarding Potential Analyzer provides data for direct calculation of $(1-\beta)$, average voltage utilization. Current utilization efficiency may be measured with a Faraday probe. Also, optical emission spectroscopy may be applied to learn about the thermodynamic state of the propellant jet.

High power thrusters have significantly higher propellant and voltage utilization efficiencies. Current utilization efficiency is similar in the high and low power thrusters. At their optimum operating points all Hall thrusters appear to require ~ 10% to 30% of the total electron flow to be recycled through the plasma to ionize neutrals and to sustain dissipative plasma processes. This recycling of electrons ultimately leads to joule heating losses. It appears that overall thrust efficiencies in the neighborhood of ~ 71 to 75% that have been achieved in higher power thrusters may be nearing a practical ultimate limit because this requires that the geometric mean of the three utilization efficiencies lie between 89 and 91%.

ACKNOWLEDGEMENT

The authors acknowledge numerous insightful discussions with James Haas, Justin Koo, Michael Holmes, and Bryan Reid that contributed to the development of the ideas and concepts presented in this paper. Professor Brad King, Jerry Ross, and Jason Sommerville provided valuable insights that led to accounting for the ionization energy loss in terms of a reduction in current utilization efficiency.

REFERENCES

[1]Zhurin, V. V., Kaufman, H. R., and Robinson, R. S., "Physics of closed drift thrusters," *Plasma Sources Sci. Technol*., Vol. 8, 1999, pp. R1-R20.

[2]Raitses, Y., Ashkenazy, J., and Guelman, M., "Propellant Utilization in Hall Thrusters," *J. Propulsion and Power*, Vol. 14, No. 2, 1998, pp. 247-253.

[3]Linnell, J. A., and Gallimore, A.D., "Efficiency Analysis of a Hall Thruster Operation with Krypton and Xenon," *J. Propulsion and Power*, Vol. 22, No. 6, 2003, pp. 1402-1412.

[4]Hofer, R. R., "Development and Characterization of High-Efficiency, High Specific Impulse Xenon Hall Thrusters," PhD Dissertation, University of Michigan, Ann Arbor, Michigan. Published as NASA/CR-2004-213099, Glenn Research Center, June 2004.

[5]Hofer, R. R., Haas, J. M., and Gallimore, A. D., "Ion voltage diagnostics in the far-field plume of a high-specific impulse Hall Thruster," 39th AIAA/ASME/SAE/ASEE Joint Propulsion Conference and Exhibit, 20-23 July 2003, Huntsville, AL, Paper No. AIAA 2003-4556.

[6]Jacobson, . T., and Jankovsky, R. S., "Test Results of a 200 W Class Hall Thruster," 34th AIAA/ASME/SAE/ASEE Joint Propulsion Conference and Exhibit, 13-15 July 1998, Cleveland, OH, Paper No. AIAA 1998-3792.

[7]Monheiser, J., Hruby, V., Freeman, C, Connolly, W., and Pote, B., "Development and testing of a low-power Hall Thruster System," Chapter 10 in *Micropropulsion for Small Spacecraft*, Micci, M. M., and Ketsdever, A. D., Editors, Progress in Astronautics and Aeronautics, Vol. 187, 2000.
[8]Ekholm, J. M., and Hargus, W. A. Jr., "ExB measurements of a 200 W xenon Hall Thruster," 41st AIAA/ASME/SAE/ASEE Joint Propulsion Conference and Exhibit, 10-13 July 2005, Tucson, AR, Paper No. AIAA 2005-4405.
[9]Manzella, D., and Oleson, S., Sankovic, J., Haag, T., Semenkin, A., and Kim, V., "Evaluation of Low Power Hall Thruster Propulsion," 32nd AIAA/ASME/SAE/ASEE Joint Propulsion Conference and Exhibit, 1-3 July 1996, Lake Buena Vista, FL, Paper No. 1996-2736.
[10]Gulczinski, F. S., and Gallimore, A. D., "Near-field ion energy and species measurements of a 5-kW Hall Thruster," J. Propulsion and Power, Vol. 17, No. 2, 2001, pp. 418-427.
[11]Hofer, R. R., and Gallimore, A.D., "High-specific impulse Hall Thrusters, Part 2: Efficiency Analysis," *J. Propulsion and Power*, Vol. 22, No. 4, 2006, pp. 732-740.
[12]Hargus, W. A. Jr., Meezan, N. B., and Cappelli, M. A., "The Transient Behavior of a Low Power Laboratory Xenon Hall Thruster," 33rd AIAA/ASME/SAE/ASEE Joint Propulsion Conference and Exhibit, 6-9 July 1997, Seattle, WA, Paper No. 1997-3050.
[13]Ekholm, J. M., Hargus, W. A., Larson, C. W., Nakles, M. R., and Reed, G., "Plume Characteristics of the Busek 600 W Hall Thruster," 42nd AIAA/ASME/SAE/ASEE Joint Propulsion Conference and Exhibit, 9-12 July 2006, Sacramento, CA, Paper No. 2006-4659.
[14]Personal Communication, Lawrence Byrne, Busek, Inc.
[15]Peterson, P. Y., Jacobson, D. T., Manzella, D. H., and John, J. W., " The Performance and Wear Characterization of a High-Power High-Isp NASA Hall Thruster," 41st AIAA/ASME/SAE/ASEE Joint Propulsion Conference and Exhibit, 10-13 July 2005, Tucson, AR, Paper No. AIAA 2005-4243.
[16]Hall thruster performance data from Busek Co. website: http://www.busek.com/downloads/HighPower.pdf
[17]Hill, P. G., and Peterson, C. R., "*Mechanics and Thermodynamics of Propulsion*," Addison-Wesley Publishing Company, Reading, Massachusetts, Third Printing, 1970, Chap. 13.
[18]Larson, C.W., Mead, F. B., and Knecht, S. D., "Benefit of Constant Momentum Propulsion for Large ΔV Missions – Application in Laser Propulsion," 42nd AIAA Aerospace Sciences Meeting and Exhibit, 5-8 January 2004, Reno, Nevada, Paper No. 2004-0649.

APPENDIX

Table 1. Cylindrical Hall Thruster [Raitses, Ashkenazy, Guelman, *J. Propulsion and Power* **14** (1998) 247-253]

Variable Cross-section (length = 30 cm)

cross section cm^2	V_a V	m' mg/s	I_a A	**F** mN	χ	η_{thrust}	T/P mN/kW	<**v**> km/s	E_1 $\Phi(1-\beta)\chi$	E_2 (1-r)/χ	$\Phi(1-\beta)$	(1-r)
10	300	2.16	2.02	36.0	0.880	0.495	59.4	16.7	0.630	0.786	0.715	0.692
10	300	1.84	1.69	29.1	0.843	0.453	57.3	15.8	0.567	0.799	0.672	0.674
10	300	1.53	1.37	21.6	0.777	0.37	52.4	14.1	0.452	0.818	0.582	0.636
10	300	1.29	1.17	17.2	0.745	0.326	48.9	13.3	0.403	0.809	0.541	0.603
10	300	1.04	0.93	12.6	0.693	0.275	45.3	12.1	0.334	0.823	0.482	0.570
10	300	0.88	0.80	10.1	0.670	0.242	42.0	11.5	0.301	0.805	0.449	0.539
10	250	2.16	1.92	31.1	0.819	0.466	64.7	14.4	0.564	0.826	0.689	0.677
10	250	1.84	1.65	26.1	0.801	0.449	63.4	14.2	0.546	0.822	0.682	0.658
10	250	1.53	1.34	18.9	0.753	0.348	56.4	12.3	0.415	0.839	0.551	0.632
10	250	1.29	1.10	14.9	0.702	0.316	54.6	11.6	0.365	0.866	0.520	0.608
10	250	1.04	0.82	11.1	0.653	0.289	54.0	10.7	0.312	0.928	0.477	0.606
10	250	0.88	0.68	8.6	0.617	0.25	51.0	9.8	0.262	0.955	0.424	0.589
10	200	2.16	2.02	26.1	0.787	0.39	64.6	12.1	0.496	0.787	0.630	0.619
10	200	1.84	1.66	21.2	0.768	0.369	64.0	11.5	0.452	0.816	0.589	0.626
10	200	1.53	1.30	15.6	0.713	0.306	60.1	10.2	0.352	0.868	0.494	0.619
10	200	1.29	1.01	12.0	0.681	0.277	59.6	9.30	0.294	0.942	0.432	0.642
10	200	1.04	0.73	8.6	0.615	0.245	59.2	8.28	0.233	1.051	0.379	0.647
10	200	0.88	0.61	7.0	0.585	0.231	57.9	7.98	0.217	1.066	0.371	0.623
6	300	2.16	2.06	33.9	0.806	0.43	54.8	15.7	0.558	0.771	0.692	0.622
6	300	1.84	1.72	28.0	0.791	0.412	54.2	15.2	0.525	0.785	0.663	0.621
6	300	1.53	1.37	21.4	0.757	0.363	52.0	14.0	0.443	0.820	0.585	0.620
6	300	1.29	1.28	17.8	0.754	0.319	46.2	13.8	0.432	0.739	0.573	0.557
6	300	1.04	1.01	13.0	0.703	0.267	42.7	12.5	0.355	0.753	0.504	0.529
6	300	0.88	0.85	10.0	0.670	0.222	39.2	11.3	0.291	0.762	0.435	0.510
6	250	2.16	2.03	29.5	0.773	0.397	58.1	13.7	0.508	0.782	0.657	0.604
6	250	1.84	1.67	24.7	0.766	0.396	59.0	13.4	0.490	0.809	0.639	0.619
6	250	1.53	1.39	20.0	0.758	0.378	57.7	13.1	0.466	0.810	0.615	0.614
6	250	1.29	1.12	15.7	0.743	0.34	56.0	12.1	0.401	0.848	0.540	0.630
6	250	1.04	0.94	12.0	0.705	0.294	50.9	11.5	0.363	0.811	0.514	0.572
6	250	0.88	0.74	9.0	0.660	0.249	48.7	10.2	0.284	0.876	0.431	0.578
6	200	2.16	2.03	25.0	0.753	0.357	61.6	11.6	0.457	0.781	0.607	0.588
6	200	1.84	1.68	20.6	0.744	0.345	61.5	11.2	0.428	0.806	0.575	0.600
6	200	1.53	1.36	16.3	0.739	0.319	59.9	10.6	0.386	0.827	0.522	0.611
6	200	1.29	1.05	12.6	0.713	0.291	59.7	9.75	0.323	0.900	0.453	0.642
6	200	1.04	0.87	9.6	0.666	0.256	55.3	9.26	0.292	0.878	0.438	0.585
6	200	0.88	0.70	7.3	0.639	0.218	52.3	8.34	0.236	0.922	0.370	0.589
4.5	300	2.16	2.14	32.4	0.827	0.379	50.5	15.0	0.512	0.740	0.619	0.612
4.5	300	1.84	1.75	26.6	0.791	0.366	50.6	14.5	0.474	0.772	0.599	0.611
4.5	300	1.53	1.40	21.4	0.779	0.356	51.0	14.0	0.443	0.804	0.568	0.626
4.5	300	1.29	1.23	17.8	0.765	0.333	48.3	13.8	0.431	0.773	0.563	0.592
4.5	300	1.04	1.05	13.5	0.742	0.279	42.8	13.0	0.385	0.725	0.518	0.538
4.5	300	0.88	0.89	10.2	0.722	0.222	38.2	11.6	0.306	0.725	0.424	0.523
4.5	250	2.16	2.10	29.5	0.800	0.383	56.1	13.7	0.508	0.754	0.635	0.603
4.5	250	1.84	1.67	23.7	0.774	0.365	56.8	12.9	0.450	0.811	0.581	0.628
4.5	250	1.53	1.33	19.1	0.748	0.358	57.4	12.5	0.423	0.845	0.566	0.632
4.5	250	1.29	1.12	15.5	0.733	0.33	55.0	12.0	0.391	0.843	0.534	0.618
4.5	250	1.04	0.91	12.0	0.699	0.306	53.0	11.5	0.363	0.844	0.519	0.590
4.5	250	0.88	0.73	8.5	0.632	0.226	46.7	9.68	0.255	0.886	0.403	0.560
4.5	200	2.16	2.12	24.7	0.780	0.333	58.3	11.4	0.444	0.750	0.569	0.585
4.5	200	1.84	1.66	20.0	0.753	0.328	60.2	10.9	0.404	0.812	0.536	0.612
4.5	200	1.53	1.32	16.1	0.722	0.319	60.7	10.5	0.375	0.850	0.520	0.614
4.5	200	1.29	1.06	12.8	0.708	0.296	59.9	9.88	0.332	0.891	0.469	0.630
4.5	200	1.04	0.81	9.5	0.654	0.268	58.6	9.15	0.285	0.941	0.435	0.615
4.5	200	0.88	0.61	7.2	0.617	0.241	58.9	8.19	0.228	1.057	0.370	0.652

Variable Length (Cross-section = 10 cm^2)

L cm	V_a V	m' mg/s	I_a A	**F** mN	χ	η_{thrust}	T/P mN/kW	<**v**> km/s	E_1 $\Phi(1-\beta)\chi$	E_2 (1-r)/χ	$\Phi(1-\beta)$	(1-r)
30	300	2.16	2.02	36.0	0.881	0.496	59.5	16.7	0.631	0.786	0.716	0.692
30	300	1.84	1.67	29.1	0.841	0.46	58.1	15.8	0.569	0.809	0.676	0.680
30	300	1.53	1.34	21.6	0.776	0.379	53.8	14.1	0.450	0.842	0.580	0.653
30	300	1.29	1.18	17.2	0.745	0.324	48.7	13.3	0.402	0.806	0.540	0.600
30	300	1.04	0.92	12.6	0.695	0.278	45.7	12.2	0.335	0.829	0.482	0.576
30	300	0.88	0.80	10.0	0.672	0.239	42.0	11.4	0.294	0.813	0.437	0.546
30	250	2.16	1.92	31.1	0.820	0.466	64.7	14.4	0.564	0.826	0.688	0.678
30	250	1.84	1.65	26.1	0.803	0.448	63.3	14.2	0.546	0.821	0.680	0.659
30	250	1.53	1.35	18.9	0.748	0.345	56.0	12.3	0.414	0.834	0.553	0.624
30	250	1.29	1.11	15.0	0.702	0.313	53.9	11.6	0.367	0.853	0.523	0.599
30	250	1.04	0.82	11.1	0.655	0.289	54.0	10.7	0.312	0.928	0.476	0.608
30	250	0.88	0.66	8.6	0.618	0.257	52.5	9.79	0.261	0.986	0.422	0.609
30	200	2.16	2.02	26.1	0.788	0.388	64.3	12.1	0.495	0.784	0.628	0.618
30	200	1.84	1.66	21.2	0.769	0.37	64.1	11.5	0.453	0.816	0.589	0.628
30	200	1.53	1.30	15.6	0.715	0.305	59.8	10.2	0.354	0.862	0.495	0.616
30	200	1.29	0.98	11.9	0.682	0.279	60.5	9.23	0.290	0.963	0.425	0.657
30	200	1.04	0.73	8.7	0.615	0.248	59.6	8.33	0.236	1.052	0.383	0.647
30	200	0.88	0.60	7.0	0.576	0.233	58.2	8.00	0.218	1.070	0.378	0.616
40	300	2.16	1.99	34.5	0.837	0.462	57.9	16.0	0.578	0.799	0.691	0.669
40	300	1.84	1.73	29.1	0.827	0.445	56.2	15.8	0.569	0.782	0.688	0.647
40	300	1.53	1.45	22.9	0.820	0.392	52.4	15.0	0.507	0.773	0.619	0.634
40	300	1.29	1.21	18.7	0.799	0.372	51.3	14.5	0.476	0.781	0.596	0.624
40	300	1.04	0.93	14.3	0.783	0.353	51.2	13.8	0.432	0.818	0.551	0.640
40	300	0.88	0.78	10.5	0.700	0.269	44.9	12.0	0.325	0.827	0.464	0.579
40	250	2.16	1.86	29.9	0.799	0.446	64.3	13.9	0.523	0.852	0.655	0.681
40	250	1.84	1.64	25.3	0.795	0.425	61.7	13.8	0.516	0.824	0.649	0.655
40	250	1.53	1.33	19.9	0.785	0.389	59.8	13.0	0.461	0.844	0.587	0.663
40	250	1.29	1.14	16.7	0.755	0.377	58.3	12.9	0.455	0.829	0.602	0.626
40	250	1.04	0.85	12.7	0.720	0.364	59.5	12.2	0.407	0.894	0.565	0.644
40	250	0.88	0.68	9.2	0.665	0.283	53.9	10.5	0.300	0.944	0.451	0.628
40	200	2.16	1.94	25.0	0.769	0.374	64.5	11.6	0.457	0.818	0.594	0.629
40	200	1.84	1.65	20.7	0.769	0.352	62.7	11.2	0.429	0.821	0.558	0.631
40	200	1.53	1.34	16.6	0.758	0.335	61.8	10.8	0.400	0.837	0.528	0.635
40	200	1.29	1.02	13.2	0.734	0.333	65.0	10.2	0.357	0.932	0.487	0.684
40	200	1.04	0.74	10.0	0.680	0.325	67.5	9.63	0.315	1.030	0.464	0.701
40	200	0.88	0.66	7.9	0.620	0.265	59.4	8.92	0.271	0.978	0.437	0.606
20	300	2.16	2.02	32.9	0.815	0.415	54.4	15.2	0.527	0.787	0.647	0.641
20	300	1.84	1.61	27.0	0.792	0.41	55.9	14.7	0.487	0.841	0.615	0.666
20	300	1.53	1.35	21.1	0.765	0.358	52.0	13.8	0.431	0.832	0.563	0.636
20	300	1.29	1.16	16.7	0.712	0.308	47.7	12.9	0.378	0.814	0.531	0.580
20	300	1.04	0.89	11.5	0.652	0.236	42.8	11.0	0.276	0.855	0.423	0.557
20	300	0.88	0.71	9.0	0.615	0.217	42.4	10.2	0.238	0.913	0.387	0.561
20	250	2.16	1.96	29.9	0.785	0.424	61.2	13.9	0.523	0.810	0.667	0.636
20	250	1.84	1.58	24.5	0.759	0.414	62.1	13.3	0.483	0.857	0.637	0.650
20	250	1.53	1.29	18.2	0.725	0.334	56.2	11.9	0.384	0.869	0.530	0.630
20	250	1.29	1.08	13.8	0.665	0.275	51.3	10.7	0.313	0.880	0.470	0.585
20	250	1.04	0.80	10.0	0.607	0.241	50.2	9.60	0.251	0.961	0.413	0.583
20	250	0.88	0.64	8.0	0.570	0.228	50.3	9.07	0.224	1.018	0.393	0.580
20	200	2.16	1.98	24.0	0.750	0.338	60.8	11.1	0.421	0.803	0.561	0.603
20	200	1.84	1.57	19.5	0.710	0.33	62.2	10.6	0.383	0.862	0.539	0.612
20	200	1.53	1.26	15.0	0.678	0.293	59.8	9.81	0.327	0.896	0.483	0.607
20	200	1.29	1.00	11.6	0.661	0.26	58.0	8.96	0.273	0.951	0.413	0.629
20	200	1.04	0.71	8.0	0.575	0.214	55.8	7.67	0.200	1.070	0.348	0.615
20	200	0.88	0.58	6.1	0.540	0.185	53.1	6.97	0.165	1.119	0.306	0.604